A MATLAB Toolbox for Estimating the Second Moments of Earthquake Ruptures

Jeffrey J. McGuire

Dept. of Geology and Geophysics, Woods Hole Oceanographic Institution, Woods Hole MA 02543

Abstract

I present a set of routines in MATLAB for estimating the second degree moments of an earthquake's rupture from far field body waves. The second moments describe the length, width, duration and directivity of a rupture. The second moments approach is particularly useful when a seismic dataset is dense enough to resolve the primary finite source properties but the geodetic data needed for a well resolved finite fault inversion are not available. In particular for M3-6 earthquakes, this approach can be a useful way to estimate rupture area without the assumptions of typical corner-frequency approaches. The provided software utilizes Empirical Green's Function deconvolution to isolate the Apparent Source Time Function (ASTF) for each station and phase. The spatial variations in the duration of the ASTF are quantified and inverted for the second moments. The inverse problem is solved using Matlab's convex optimization routines for systems of linear matrix inequalities. An error analysis using the jackknife and bootstrap methods is included. An example M_w 4.7 earthquake from the San Jacinto Fault is used to demonstrate the method.

1 Introduction

The second moments of the slip-rate distribution for any earthquake describe the spatial and temporal extent of the rupture as well as its propagation, all of which contribute

to the apparent duration of the earthquake observed in any particular far-field phase. For an earthquake with a constant moment tensor such that the spatial variations in moment-rate are described by:

$$\underline{\underline{\dot{M}}}(\underline{x},t) = \underline{\underline{\hat{M}}}\dot{f}(\underline{x},t) \tag{1}$$

The second moments are defined as:

$$\begin{aligned}
\hat{\boldsymbol{\mu}}^{(2,0)} &= \int\int \dot{f}(\boldsymbol{r},t)(\boldsymbol{r}-\boldsymbol{r}_0)(\boldsymbol{r}-\boldsymbol{r}_0)dVdt \\
\hat{\mu}^{(0,2)} &= \int\int \dot{f}(\boldsymbol{r},t)(t-t_0)(t-t_0)dVdt \\
\hat{\boldsymbol{\mu}}^{(1,1)} &= \int\int \dot{f}(\boldsymbol{r},t)(\boldsymbol{r}-\boldsymbol{r}_0)(t-t_0)dVdt
\end{aligned} \tag{2}$$

where $\dot{f}(\boldsymbol{r},t)$ is a scalar function that describes the spatial and temporal distribution of moment release along the fault (*McGuire et al.*, 2001), $\boldsymbol{r}_0$ and t_0 denote the centroid location and time (i.e. the first moments) respectively. The hat denotes that these are central moments taken about the centroid. The integrals are taken over the entire source volume and earthquake duration (*Backus*, 1977a,b; *McGuire et al.*, 2001).

When $\dot{f}(\boldsymbol{r},t)$ is integrated over the volume of the source, it is known as the moment-rate or source time function (STF) $\dot{M}(t)$. The second spatial moment $\hat{\boldsymbol{\mu}}^{(2,0)}$, is related to the spatial extent of the rupture area, the second temporal moment $\hat{\mu}^{(0,2)}$ is related to the duration of rupture, and the mixed moment $\hat{\boldsymbol{\mu}}^{(1,1)}$ is related to rupture propagation.

There is considerable background literature on second moments. In general they are a way to capture the overall kinematic properties of a rupture that are well constrained by the far-field waveforms. For a more detailed theoretical background and examples in various settings, see: *Backus and Mulcahy* (1976a,b); *Backus* (1977a,b); *Bukchin* (1995); *Clévédé et al.* (2004); *Das and Kostrov* (1997); *Doornbos* (1982a,b); *Gusev and Pavlov* (1988); *McGuire et al.* (2001); *Silver* (1983). This toolbox mostly follows the measurement scheme developed in *McGuire* (2004) and the inversion scheme developed initially in *McGuire et al.* (2001). The measurement scheme and partial derivatives are specific to far-field body waves with some sort of time domain Green's function available

for propagation corrections (empirical or theoretical). For surface-wave based schemes the inversion algorithms still apply but a different measurement and partial derivative calculation scheme is required depending on the approach (see *McGuire et al.* (2001), *Clévédé et al.* (2004), *Chen et al.* (2005), and *Llenos and McGuire* (2007)).

The characteristic rupture duration τ_c, rupture length L_c, and average propagation velocity of the instantaneous spatial centroid $\boldsymbol{v_0}$ are defined following *Backus and Mulcahy* (1976a), *Backus* (1977a), *Silver and Jordan* (1983) *Silver* (1983) and *McGuire et al.* (2001):

$$\begin{aligned} x_c(\hat{\boldsymbol{n}}) &= 2\sqrt{\hat{\boldsymbol{n}}^T \hat{\boldsymbol{\mu}}^{(2,0)} \hat{\boldsymbol{n}}} \\ \tau_c &= 2\sqrt{\hat{\mu}^{(0,2)}} \\ v_c &= L_c/\tau_c \\ \boldsymbol{v}_0 &= \hat{\boldsymbol{\mu}}^{(1,1)}/\hat{\mu}^{(0,2)} \end{aligned} \tag{3}$$

where x_c is the spatial extent of the rupture in the direction $\hat{\boldsymbol{n}}$ and L_c is the maximum value of x_c (i.e. corresponding to the largest eigenvalue of $\hat{\boldsymbol{\mu}}^{(2,0)}$). W_c corresponds to the second largest eigenvalue, e.g. the rupture width. The second moments can either be calculated in three spatial dimensions or along a 2D fault-plane if the mechanism is known. To resolve the fault plane ambiguity, we typically invert for the second moments assuming each 2D nodal plane and choose the one with the higher variance reduction as the true nodal plane.

In general the characteristic dimensions give an idea of the region that contributed substantially to moment-relase and the relative importance of directivity in the rupture. Figure 1 shows an example of the characteristic dimensions calculated for a theoretical crack model with unilateral propagation from *Kaneko and Shearer* (2015). The ellipse defined by the second spatial moment captures the orientation and extent of the region with the large slip, which is smaller than the total dimension of the rupture (Figure 1). Similarly the second temporal moment captures the time period in which most of the moment was released, not the total duration (Figure 1). This definition of earthquake duration is theoretically closely related to the corner-frequency obtained from simple

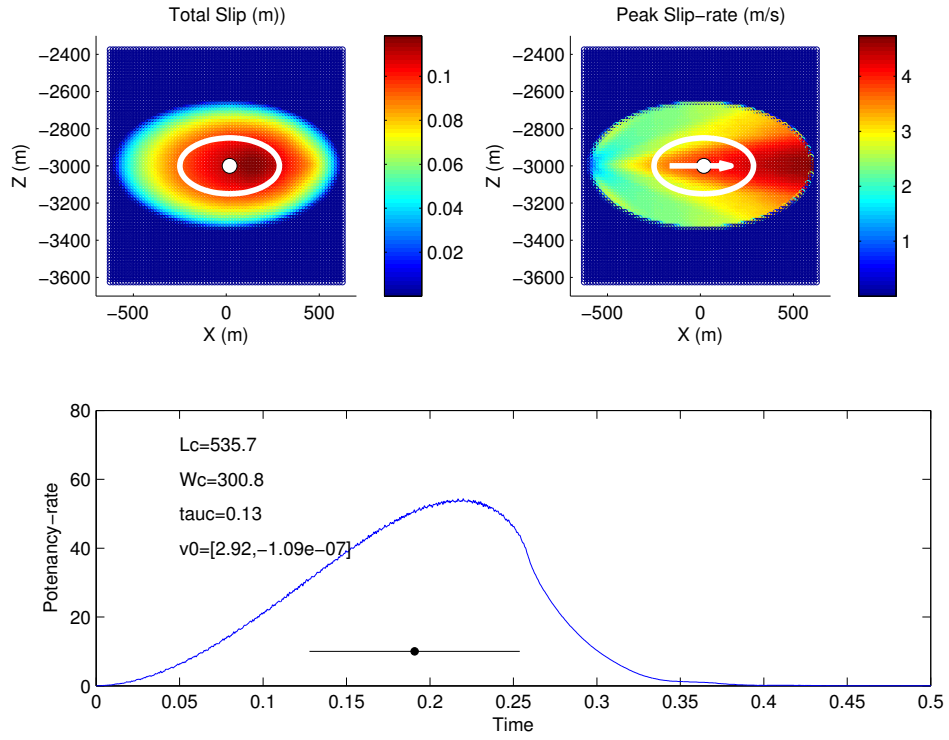

Figure 1: An Elliptical source from *Kaneko and Shearer* (2015), (their Figure 10). Top Left) Slip distribution. The white ellipse has major axis of length L_c and minor axis W_c. Top Right The spatial distribution of the peak slip-rate. The rupture propagated unilaterally from left to right and in this model the slip-rate is highest at the righthand edge. The vector shows the mixed moment $\hat{\boldsymbol{\mu}}^{(1,1)}$ scaled to the distance L_0. Bottom, The potency-rate for the modeled rupture (blue line). The black circle gives the centroid time, and the horizontal line through it has a length equal to τ_c to illustrate the difference between τ_c and the total duration. The values for L_c and W_c are given in meters, τ_c in seconds, and v_0 in km/s. v_0 has components in the along-strike direction and the downdip direction.

spectral fitting (*Silver*, 1983), but in practice the second moments may result in better estimates of rupture area (*Chen and McGuire*, 2016).

2 Software Requirements

The toolbox contains three main directories. The **src** directory contains the MATLAB functions for making measurements and inversion as well as a fortran program for calculating takeoff angles. The **SJFex** directory contains an example M_w 4.7 earthquake from the San Jacinto Fault in southern California. The third directory contains a pdf of this manual. To use this toolbox you need only the codes in the **src** directory

and MATLAB. The inversion algorithm uses some routines from MATLAB's Robust Control toolbox.

3 Data Preparation

The input to the EGF algorithm is simply pairs of velocity seismograms for each station/component that you would like to try a deconvolution on. The code is currently set up to allow interactive waveform windowing, this could be automated if you prefer. The SJFexamp directory contains an example of the data preparation using event directories of miniseed files and the Antelope software package for event information. The data loading is done in the script runSJFsetup.m which could be easily modified to match other databasing approaches.

The example event is a M_w 4.7 earthquake on March 11th 2013 that was recorded by both the ANZA network and a dense temporary deployment of instruments including numerous strong motion sensors (*Kurzon et al.*, 2014). The example event is run with the runSJFex.m script. The flag LOADDATAFILE can be set to 1 to use a pre-loaded .mat file with all of the necessary arrays, or it can be set to 0 to load the miniseed files and alter filters, etc. If loading directly from miniseed, the key choices to make are the 'dofilt' flag, and $fmin$ and $fmax$ which collectively set the frequency bandpass for filtering the data. The code is setup to integrate all seismograms with component names like 'HNZ' from acceleration to velocity. The key choice is specifying the list of stations and components to be read in/tried for deconvolutions. This is done in the stasm and compm variables. This could be automated to look for all pairs in the event and egf directories.

4 Measurements

Our approach requires using the far-field body wave data to estimate the moment-rate function from the P and/or S wave at a set of azimuthally distributed stations. This

estimate will be either a stretched or compressed version of the true moment rate function due to the finite source properties of the rupture and hence is termed an Apparent Source Time Function (ASTF). Because many moderate earthquakes require working at relatively high-frequencies (>1 Hz) to retrieve the ASTF, we typically use Empirical Green's Functions (EGFs) to remove propagation effects. Many EGF deconvolution algorithms, such as the water-level technique, produce ASTF estimates that have low-amplitude ringing for an extended period of time following the main pulse of moment release that make it difficult to determine the end of the rupture. One technique that provides an objective determination of the duration of the ASTF is the projected Landweber deconvolution (PLD) algorithm of *Bertero et al.* (1997) and *Lanza et al.* (1999). This algorithm performs the deconvolution with moment release restricted to a series of increasing-length time intervals and analyzes the misfit as a function of the interval length (see Fig. 2). The interval length where this trade-off curve flattens out is chosen as the interval during which moment release is allowed (*Lanza et al.*, 1999). This technique produces ASTFs that satisfy a positivity constraint, provide a good fit to the observed seismograms, and are very consistent between nearby stations (*McGuire*, 2004).

The matlab files for making the measurements are:

- *makemeasurements.m* This contains the GUI for looping through velMS and velEGF arrays and making the measurements of $\mu^{(0,2)}(\underline{s})$.
- *pld.m* This file contains the implementation of the projected Landweber deconvolution algorithm. The key control parameter for the deconvolution is the number of iterations. Effectively, the higher this number (variable niter), the better the ASTF will do at fitting the highest frequency energy in the mainshock waveform. It is best to experiment with a range of values for your dataset, starting relatively low (10, 50) and increasing. Typically a value of 100 is a good compromise between seismogram fit and computation time.
- $findt2.m$ calculates $\mu^{(0,2)}(\underline{s})$ for the ASTF that results from the deconvolution.

This gives you the option to pick the starting and ending time points of the ASTF that you want to include in the calculation. Assuming this is working well, this choice could be omitted (set pickt2=0) and the calculation will be done on the entire range of the time function.

The flag DOMEAS lets you choose between either just loading in an example set of measurements or going through the process of making the measurements yourself.

In making the measurements, the routine is set to store the current set of measurements after each station in the file measurements.mat. This is intended to allow you to stop part way through a dataset and restart at a later time or simply go back and revise a few stations that appear to need it after seeing the whole dataset. The first window that appears asks you if you want to load an existing set of measurements from this file or start from scratch. The *makemeasurements.m* function will loop through all of the channels in the dataset and ask you to make a series of choices for each:

- The first menu ask you if you want to start a new set of measurements or load the previous set from MEASUREMENTS.mat. The script will save the measurements you've made after each station. This provides an easy way to stop in the middle and restart later. The MEASUREMENTS.mat file is overwritten after every station is processed, so if you wish to save it, you need to copy it to some other filename. If this is your first attempt with this event, choose 'Start New' to initialize the variables.

- The first plot shows the MS and EGF waveforms and ask you if this channel is worthy of doing a deconvolution. If you say no, DONE(i) remains =0 and this channel will not be used. If you choose yes, you will move onto windowing the MS and EGF waveforms.

- If you choose to try deconvolving this channel, it will ask you to manually pick a time range to zoom in on the mainshock waveform. Just click roughly before the beginning of the P or S phase that you want to work on. It will then replot this time range of the MS and ask you to pick the time range to be fit by the

deconvolution. It is best to pick a window surrounding the 'main arrival'. The inversion assumes that the ASTF reflects energy that left the source at roughly the slowness vector of the first arrival. So it is most accurate to not try and fit the later parts of the coda which likely reflect different slownesses. In practice, we usually pick the start of the interval as being 20-50 samples before the first arrival (e.g. so there is a relatively flat, near-zero, part before the arrival). Picking the end of the fitting interval can be tricky. Ideally, the waveform would've returned to near-zero amplitude relatively quickly after the main arrival. For a M4-5 earthquake we typically fit 3-5 seconds of P or S-wave. If there is a clear second arriving phase (Pn, etc) it is best to end the interval before that arrival. For stations with a strong coda, it is often very difficult to pick the end of the interval. These stations will often not work very well.

- Once the MS fitting interval has been picked, it will replot this interval and ask you to pick the onset time of the P or S wave.
- It will then plot the EGF waveform and ask you for a interval to zoom into. This is slightly different. You should zoom fairly tightly on the first arrival. It will then replot this window and ask you to pick the first arrival time, which defines the start of the Green's function.
- Once the waveforms have been picked, it will perform the PLD for a series of allowed durations of the ASTF and calculate the misfit for each deconvolution. It will plot this tradeoff curve (misfit vs ASTF interval). If the EGF was a good choice, then the tradeoff curve will have a region where it drops steadily to a low value ($\leq .3$) and then flattens out. In a ideal case there is a clear break in slope of the tradeoff curve that identifies the correct value for the total duration at that station. It will ask you to pick this inflection point. See Figure 2 for some examples.
- if you have set the flag pickT2=1 it will plot the ASTF for your choice and ask you to pick the start and end points for the integration that calculates $\mu^{(0,2)}(\underline{s})$. This

is sometimes desirable for earthquakes that do not end abruptly in case you want to revise your choice without re-doing the deconvolution. If you had pickT2=0, then it does this calculation automatically on the whole ASTF (usually fine for good datasets).

- It will now plot the ASTF and the fit to the data and ask you to choose among 4 options for saving the result; Finished P-wave, Finished S-wave, re-do, or "No, done" on this channel and move on to the next. The first two set the DONE variable to 1 for this channel and record wether it was a P or S wave. re-do lets you go through this channel again in case you think you got the windowing wrong. The "No,done" option will set the $DONE$ variable to zero and this channel will not be used in the inversion.
- the script will loop through this process for the rest of the stations

Once this loop has been completed for all stations and the $DONE$ variable has been set to 1 or 0 for each the measurement process is complete and saved.

5 Inversion Scheme for Second moments

The inversion algorithm is essentially identical to that in *McGuire* (2004) and *McGuire et al.* (2001) but has been implemented using the Robust Control toolbox in Matlab. In general the inverse problem for the second moments can be posed as a simple linear inversion based on the equation for the observations

$$\mu^{(0,2)}(\underline{\mathbf{s}}) = \hat{\mu}^{(0,2)} - 2\underline{\mathbf{s}} \cdot \underline{\hat{\mu}}^{(1,1)} + \underline{\mathbf{s}} \cdot \underline{\underline{\hat{\mu}}}^{(2,0)} \cdot \underline{\mathbf{s}} \tag{4}$$

where $\underline{\mathbf{s}}$ is the slowness vector associated with a particular measurement. See *Silver* (1983) and *McGuire* (2004) for details. However, in practice if the station distribution is suboptimal, this could result in unphysical estimates for the second moments (*Das and Kostrov*, 1997). We always enforce the constraint that the source region have non-negative volume (*McGuire et al.*, 2001) which is accomplished by enforcing the

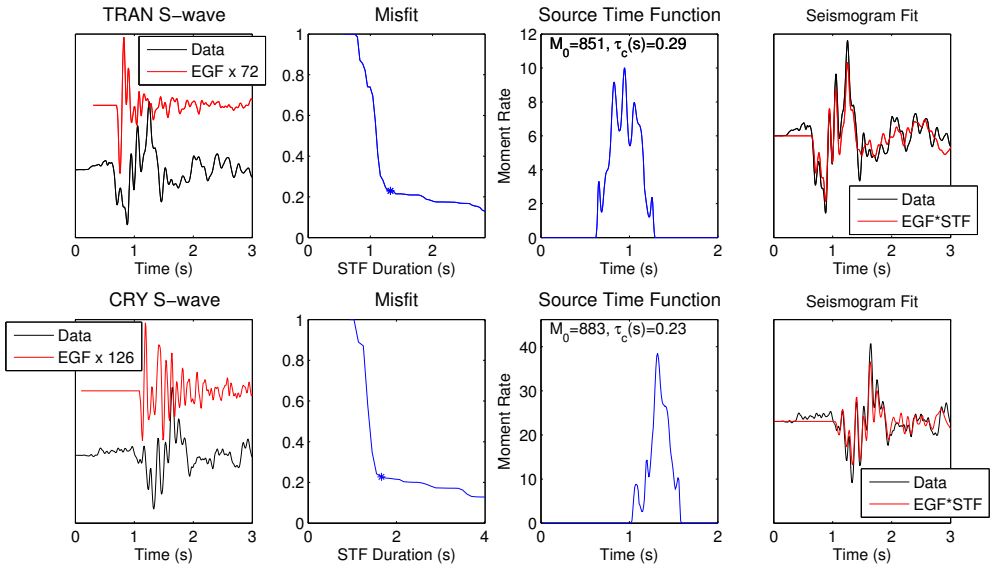

Figure 2: Examples of the EGF deconvolution measurements from the M5.1 March 2013 earthquake on the San Jacinto Fault for the S-waves recorded at stations TRAN (top row) and CRY (bottom row). The left panels show the raw velocity seismograms for the M5.1 and an EGF event. The next panel shows the tradeoff curve for waveform misfit versus source time function duration with the asterisks denoting our pick for the duration of the moment-rate function as seen by that S-wave. The third panels show the resulting moment-rate function (in units of the EGF event's moment). The fourth panels show the fit to the mainshock seismograms. Station TRAN sees a slightly longer ASTF (characteristic duration of 0.29 s) than CRY (0.23 seconds).

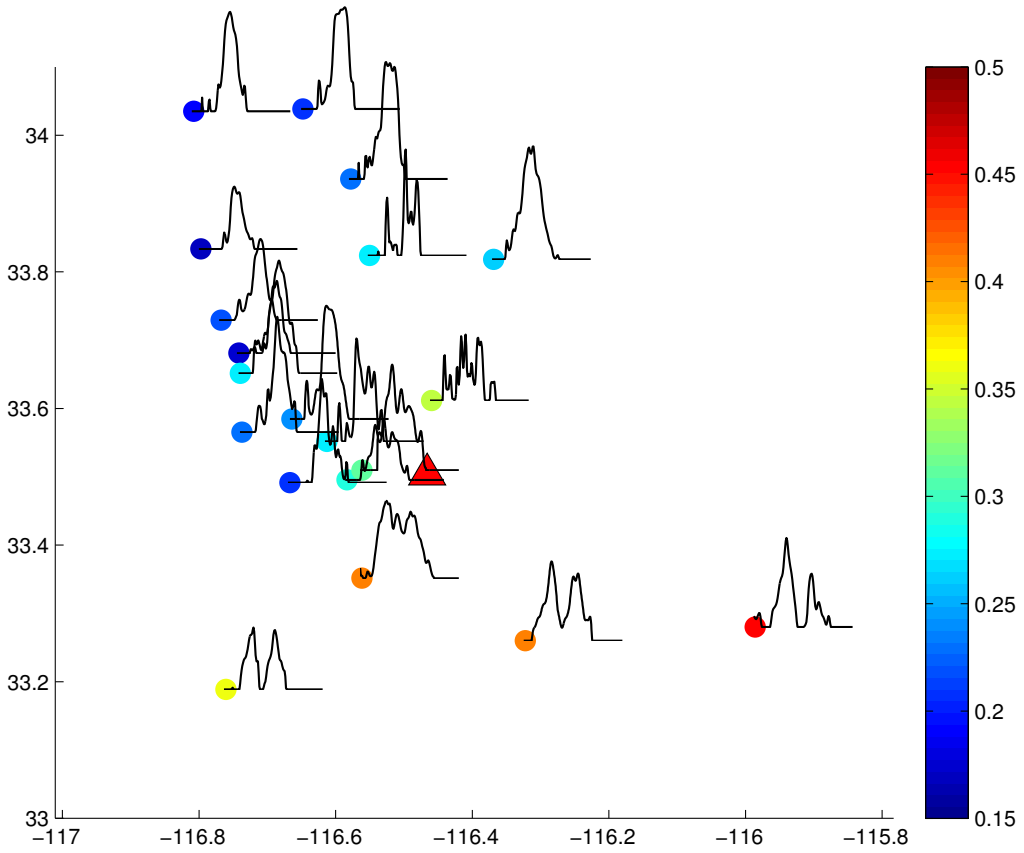

Figure 3: ASTFs resulting from EGF deconvolutions at stations in the SJFZ array as a result of the March 2013 M5.1 earthquake (red triangle). Each ASTF is plotted at the location of the station denoted by the circle. The colorscale of the circles denotes the characteristic duration of that moment-rate function, $\tau_c(s)$, in seconds. The earthquake lasted about 0.3 seconds but appears longer to the SW and shorter to the NE.

matrix inequality:

$$\begin{bmatrix} \hat{\mu}^{(\mathbf{2},\mathbf{0})} & \hat{\mu}^{(\mathbf{1},\mathbf{1})^{\mathrm{T}}} \\ \hat{\mu}^{(\mathbf{1},\mathbf{1})} & \hat{\mu}^{(0,2)} \end{bmatrix} \geq 0, \tag{5}$$

where ≥ 0 indicates that the matrix is required to be positive semi-definite.

To set up an inverse problem based on equation 4, we simply need the measurements of $\mu^{(0,2)}(\underline{\mathbf{s}})$ from the previous section and the corresponding slowness vectors for each phase. We include a fortran program for calculating the takeoff angles that is run external to matlab called topp. Most of this code is taken directly from the hypoDD software package of *Waldhauser and Ellsworth* (2000). See http://earthquake.usgs.gov/research/software/. *topp* is called from within the subroutine for calculating the partial derivatives.

[G]=getpartials_2d_generic(mlats,mlons,melevs,late,lone,depe,Vp,Vs,topl,phas,strike,dip);

where *mlats*, *mlons*, and *melevs* give the station coordinates, *late*, *lone*, *depe* give the earthquake coordinates, Vp, Vs, and *topl* give the layered velocity model and topl is the depth of the top of each layer in km. *phas* is a character array the length of the number of measurements that has either the value P or S for each measurement. This routine calculates the partial derivatives for a 2-D source along a fault specified by *strike* and *dip* in the usual convention.

If the DOINVERSION flag is set to 1, the runSJFex script will call the function seconds_2d_v2.m to do the actual inversion. To solve equation 2 in a least-squares sense subject to equation 3, we recast equation 2 as a linear matrix inequality, similar to equation 3, and solve the system using Matlab's Robust Control toolbox. The least-squares problem from equation 2 is rewritten $||Ax-b|| \leq c$ where c is a dummy decision variable. The problem in LMI form is then given by:

minimize c

$$\text{subject to} \quad \begin{bmatrix} c & \mathbf{Ax}-\mathbf{b} \\ (\mathbf{Ax}-\mathbf{b})^{\mathrm{T}} & \mathbf{I}^N \end{bmatrix} \geq 0\,, \tag{6}$$

$$\text{and} \quad \begin{bmatrix} \hat{\mu}^{(2,0)} & \hat{\mu}^{(1,1)^{\mathrm{T}}} \\ \hat{\mu}^{(1,1)} & \hat{\mu}^{(0,2)} \end{bmatrix} \geq 0\,,$$

$$\text{and} \quad \hat{\mu}^{(0,2)} \leq \max(\mathrm{b})$$

where $\mathbf{I}^N$ is the identity matrix with dimension equal to the number of measurements, N, and ≥ 0 indicates the matrix is positive semidefinite. The equivalence between the linear least-squares problem and the above can be seen by calculating the eigenvalues of the $N+1$ by $N+1$ matrix, which are non-negative when the matrix is positive semi-definite. This restatement of the problem is known as using Schur complements to represent a nonlinear constraint as linear matrix inequality (*Vandenberghe and Boyd*, 1996). The last equation ensures that the estimate of the second temporal moment is smaller than the largest measurement of $\mu^{(0,2)}(\underline{\mathbf{s}})$, which should be true for any dataset that contains stations with good azimuthal coverage.

MATLAB's robust control toolbox contains many routines that are particularly useful for problems with matrix inequality constraints like (5). For a detailed description of how to use these, see the MATLAB manual pages. The script *seconds_2d_v2.m* shows how to implement the problem in (6) within MATLAB's LMI syntax. For each matrix inequality, the matrix on the lefthand side is first defined in terms of the optimization variables (the second moments) using the function *lmivar*. Each individual inequality in (6) is added to the LMI system using the function *lmiterm*. For instance, the lines:

```
[Xposvolume,NDEC,XDEC]=lmivar(type,struct);
lmiterm([-1 1 1 Xposvolume], 1, 1);
```

is an implementation of equation (5) where the variable $\mathbf{X_{posvolume}}$ represents the LHS :

$$\mathbf{X_{posvolume}} = \begin{bmatrix} \hat{\mu}^{(\mathbf{2,0})} & \hat{\mu}^{(\mathbf{1,1})^{\mathrm{T}}} \\ \hat{\mu}^{(\mathbf{1,1})} & \hat{\mu}^{(0,2)} \end{bmatrix} \geq \mathbf{0}, \tag{7}$$

and $\mathbf{X_{posvolume}}$ has been previously specified as a 3 by 3 symmetric matrix composed of the six independent elements of the second moments (for a 2D fault) which we seek to estimate with the MATLAB to solver. The LMI is described to MATLAB by specifying the location of each individual term within the LMI by which side of the inequality it is on, which entry within the matrix it is part of, and any constant factors that multiply it. The entries in the call to *lmiterm* are the *termid*, and two constant matrices A and B (see the *lmiterm* man pages). The LMI we are describing has only one term on the LHS and it is a matrix variable type of term. It has no pre or post multiplying matrices so A and B are set equal to 1. For the *termid* = [-1 1 1 $\mathbf{X_{posvolume}}$], the entries are:

- first entry = -1 denotes the sign of the inequality in MATLAB's convention (-1 indicates the greater side of the inequality) and that this is the first constraint equation (they are concatenated into a block diagonal system).
- second and third entries =1 give the location of the next variable in the matrix (e.g., there is only 1,1 in this example).
- fourth entry =$\mathbf{X_{posvolume}}$ is the term to be added to the location specified in the LMI.

Note that a sequence of LMIs such as (6) is implemented as one block diagonal LMI, so the first entry is incremented (1,2,3,...) in seconds_2d_v2.m to accommodate each subsequent constraint equation as a new block.

6 Error Analysis

We present two versions of error analysis that have been used previously in second moment studies based on the Jackknife and Bootstrap approaches. Both approaches

are based on resampling the data vector. Often seismic arrays involve a number of stations that are located close together while other parts of the focal sphere are poorly sampled at best. Thus, it is not straight forward to apply techniques like the Jackknife that assume each data point is independent. In our case, nearby station will likely have highly correlated measurements both in terms of the true values of $\tau_c(s)$ and the errors introduced by imperfect EGFs. To account for this when sub-sampling the dataset, we delete all of the stations in an azimuthal bin, typically with a range of 20° to 40°. The Jackknife calculation produces an estimate of the covariance matrix of the six second moment quantities from which errors on the derived characteristic rupture quantities can be estimated (*McGuire et al.*, 2001). The jacknknife calculation with 20 degree azimuth bins results in the following 1σ error estimates for the San Jacinto fault example in Figures 2 and 3: $\tau_c = 0.30 \pm 0.015s$, $L_c = 0.33 \pm 0.06km$, $W_c = 0.19 \pm 0.12km$, $V_0 = [0.84, 0.58] \pm [0.03, 0.26]km/s$.

In general, the Jackknife results are sufficient to capture the uncertainty. It is sometimes worthwhile to perform inversions for a number of random perturbations to the earthquake location, velocity model, or fault plane orientation if the uncertainties in those quantities are well known to evaluate their influence (*McGuire*, 2004). Another interesting approach is to apply the bootstrap technique. The boot strap approach with 1000 resamples of the data vector (with replacement) yields the PDFs for τ_c and Ł$_c$ shown in Figure 4. As can be seen in Figure 4, the Jackknife error bounds capture well the peaks of the bootstrap PDFs for L_c and τ_c. However, when there are only a small number of stations in a critical azimuth (e.g. the forward or backward rupture directions), then the resamples that lack stations from this direction can result in values that are well outside the Jackknife bounds. In particular, for the San Jacinto earthquake, there are only three stations that capture the long durations in the backward direction. For resamples that do not involve these observations, there is much greater variability in the second moment estimates as would be expected. The 95% confidence limits from the bootstrap are $[0.25, 0.36]$ and $[0.31, 1.39]$ km for τ_c and L_c respectively. The extent to which these are meaningful depends on how dense the

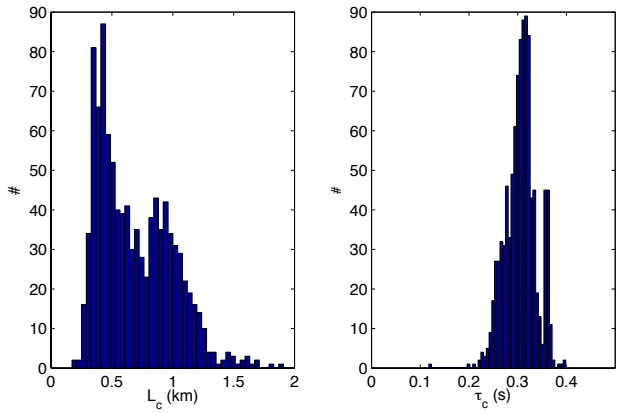

Figure 4: Examples of 1000 runs of the bootstrap calculation for the San Jacinto fault example in Figures 2 and 3 for the estimates of τ_c and L_c.

303 station distribution is.

7 Data and Resources

Seismograms used in this study were collected as part of the ANZA Network and the San Jacinto Fault Zone PASSCAL experiment. Data can be obtained from the IRIS Data Management Center at www.iris.edu (last accessed September 2016).

8 Acknowledgements

Thanks to Yoshi Kaneko for sharing the results of his dynamic rupture simulations for calculating the second moments shown in Figure 1. Thanks to Yehuda Ben-Zion and Frank Vernon for sharing the San Jacinto fault earthquake dataset. This work was supported with SCEC grant 16104 and USGS NEHRP Award 2016-0188.

References

Backus, G., and M. Mulcahy (1976a), Moment tensors and other phenomenological descriptions of seismic sources .2. discontinuous displacements, *Geophysical Journal of the Royal Astronomical Society*, *47*(2), 301–329, doi:10.1111/j.1365-246X.1976.tb01275.x.

Backus, G., and M. Mulcahy (1976b), Moment tensors and other phenomenological descriptions of seismic sources - continuous displacements, *Geophysical Journal of the Royal Astronomical Society*, *46*(2), 341–361, doi:10.1111/j.1365-246X.1976.tb04162.x.

Backus, G. E. (1977a), Interpreting seismic glut moments of total degree 2 or less, *Geophysical Journal of the Royal Astronomical Society*, *51*(1), 1–25, doi:10.1111/j.1365-246X.1977.tb04187.x.

Backus, G. E. (1977b), Seismic sources with observable glut moments of spatial degree 2, *Geophysical Journal of the Royal Astronomical Society*, *51*(1), 27–45, doi:10.1111/j.1365-246X.1977.tb04188.x.

Bertero, M., D. Bindi, P. Boccacci, M. Cattaneo, C. Eva, and V. Lanza (1997), Application of the projected landweber method to the estimation of the source time function in seismology, *Inverse Problems*, *13*, 465–486.

Bukchin, B. G. (1995), Determination of stress glut moments of total degree-2 from teleseismic surface-wave amplitude spectra, *Tectonophysics*, *248*(3-4), 185–191, doi:10.1016/0040-1951(94)00271-a.

Chen, P., T. H. Jordan, and L. Zhao (2005), Finite-Moment Tensor of the 3 September 2002 Yorba Linda Earthquake, *Bull. Seism. Soc. Am.*, *95*, 1170–1180, doi:doi:10.1785/012004094.

Chen, X., and J. J. McGuire (2016), Measuring earthquake source parameters in the Mendocino triple junction region using a dense OBS array: Implications for fault

strength variations, *Earth and Planetary Science Letters*, *453*(1), 276 – 287, doi: http://dx.doi.org/10.1016/j.epsl.2016.08.022.

Clévédé, E., M.-P. Bouin, B. Bukchin, A. Mostinskiy, and G. Patau (2004), New constraints on the rupture process of the 1999 August 17 Izmit earthquake deduced from estimates of stress glut rate moments, *Geophysical Journal International*, *159*(3), 931–942, doi:10.1111/j.1365-246X.2004.02304.x.

Das, S., and B. V. Kostrov (1997), Determination of the polynomial moments of the seismic moment rate density distribution with positivity constraints, *Geophysical Journal International*, *131*(1), 115–126, doi:10.1111/j.1365-246X.1997.tb00598.x.

Doornbos, D. J. (1982a), Seismic moment tensors and kinematic source parameters, *Geophysical Journal of the Royal Astronomical Society*, *69*(1), 235–251, doi: 10.1111/j.1365-246X.1982.tb04946.x.

Doornbos, D. J. (1982b), Seismic source spectra and moment tensors, *Physics of the Earth and Planetary Interiors*, *30*(2-3), 214–227, doi:10.1016/0031-9201(82)90109-1.

Gusev, A. A., and V. M. Pavlov (1988), Determination of space-time structure of a deep earthquake source by means of power moments, *Tectonophysics*, *152*(3-4), 319–334, doi:10.1016/0040-1951(88)90057-1.

Kaneko, Y., and P. M. Shearer (2015), Variability of seismic source spectra, estimated stress drop, and radiated energy, derived from cohesive-zone models of symmetrical and asymmetrical circular and elliptical ruptures, *Journal of Geophysical Research: Solid Earth*, *120*(2), 2014JB011,642, doi:10.1002/2014JB011642.

Kurzon, I., F. L. Vernon, Y. Ben-Zion, and G. Atkinson (2014), Ground motion prediction equations in the san jacinto fault zone: Significant effects of rupture directivity and fault zone amplification, *Pure and Applied Geophysics*, *171*(11), 3045–3081, doi:10.1007/s00024-014-0855-2.

Lanza, V., D. Spallarossa, M. Cattaneo, D. Bindi, and P. Augliera (1999), Source parameters of small events using constrained deconvolution with empirical green's functions, *Geophysical Journal International*, *137*(3), 651–662, doi:10.1046/j.1365-246x.1999.00809.x.

Llenos, A. L., and J. J. McGuire (2007), Influence of fore-arc structure on the extent of great subduction zone earthquakes, *Journal of Geophysical Research-Solid Earth*, *112*(B9), 31, doi:B09301 10.1029/2007jb004944.

McGuire, J. J. (2004), Estimating finite source properties of small earthquake ruptures, *Bulletin of the Seismological Society of America*, *94*(2), 377–393.

McGuire, J. J., L. Zhao, and T. H. Jordan (2001), Teleseismic inversion for the second-degree moments of earthquake space-time distributions, *Geophysical Journal International*, *145*(3), 661–678.

Silver, P. (1983), Retrieval of source-extent parameters and the interpretation of corner frequency, *Bulletin of the Seismological Society of America*, *73*(6), 1499–1511.

Silver, P. G., and T. H. Jordan (1983), Total-moment spectra of 14 large earthquakes, *Journal of Geophysical Research*, *88*(NB4), 3273–3293, doi:10.1029/JB088iB04p03273.

Vandenberghe, L., and S. Boyd (1996), Semidefinite programming, *Siam Review*, *38*(1), 49–95, doi:10.1137/1038003.

Waldhauser, F., and W. L. Ellsworth (2000), A double-difference earthquake location algorithm: Method and application to the northern hayward fault, california, *Bulletin of the Seismological Society of America*, *90*(6), 1353–1368, doi:10.1785/0120000006.